ADVANCED MATERIALS INTERFACES
www.advmatinterfaces.de

Deformable and Robust Core–Shell Protein Microcapsules Templated by Liquid–Liquid Phase-Separated Microdroplets

*Yufan Xu, Yi Shen, Thomas C. T. Michaels, Kevin N. Baumann, Daniele Vigolo, Quentin Peter, Yuqian Lu, Kadi L. Saar, Dominic Vella, Hongjia Zhu, Bing Li, He Yang, Alexander P. M. Guttenplan, Marc Rodriguez-Garcia, David Klenerman, and Tuomas P. J. Knowles**

Microcapsules are a key class of microscale materials with applications in areas ranging from personal care to biomedicine, and with increasing potential to act as extracellular matrix (ECM) models of hollow organs, tissues, or biomolecular condensates. Such capsules are conventionally generated from non-ECM materials including synthetic polymers. Here, robust microcapsules with controllable shell thickness from physically- and enzymatically-crosslinked gelatin are fabricated, and a core–shell architecture is achieved by exploiting a liquid–liquid phase-separated aqueous system in a one-step microfluidic process. Microfluidic mechanical testing reveals that the mechanical robustness of thicker-shell capsules could be controlled through modulation of the shell thickness. Furthermore, the microcapsules demonstrate environmentally-responsive deformation, including buckling driven by osmosis and external mechanical forces. A sequential release of cargo species is obtained through the degradation of the capsules. Stability measurements show the capsules are stable at 37 °C for more than 2 weeks. Finally, through gel–sol transition, microgels function as precursors for the formation of all-aqueous liquid–liquid phase-separated systems that are two-phase or multiphase. These smart capsules that can undergo phase transition are promising models of hollow biostructures, microscale drug carriers, and building blocks or compartments for active soft materials and robots.

1. Introduction

Artificial protein-based systems can be harnessed to form hydrogels and colloids at the microscale. Such materials can act as powerful tools to investigate biomechanics of biomaterials, including shedding light on how cells and tissues behave with varying substrate mechanics.[1–3] Protein materials at water–water interfaces, such as all-aqueous emulsions, have been increasingly explored and thought to be associated with diseases, and notably they can confer functional advantages to the formation of next-generation soft or liquid materials.[4–9] Such studies can be crucially further advanced by extracellular matrix (ECM) protein-based materials as the components of biomimetic models in vitro. The mechanical properties and the phase characteristics of natural hydrogels play significant roles in modulating cellular function, but it has been challenging to track the deformation, the phase separation, and the phase transition of these soft materials at the microscale.[1,10,11] Small and

Y. Xu, Y. Shen, T. C. T. Michaels, K. N. Baumann, Q. Peter, Y. Lu, K. L. Saar, H. Zhu, B. Li, H. Yang, A. P. M. Guttenplan, M. Rodriguez-Garcia, D. Klenerman, T. P. J. Knowles
Yusuf Hamied Department of Chemistry
University of Cambridge
Cambridge CB2 1EW, UK
E-mail: tpjk2@cam.ac.uk
Y. Shen
School of Chemical and Biomolecular Engineering
The University of Sydney
Sydney, NSW 2006, Australia
Y. Shen, D. Vigolo
The University of Sydney Nano Institute
The University of Sydney
Sydney, NSW 2006, Australia
The ORCID identification number(s) for the author(s) of this article can be found under https://doi.org/10.1002/admi.202101071.

DOI: 10.1002/admi.202101071

T. C. T. Michaels
Paulson School of Engineering and Applied Sciences
Harvard University
Cambridge, MA 02138, USA
K. N. Baumann, T. P. J. Knowles
Cavendish Laboratory
University of Cambridge
Cambridge CB3 0HE, UK
D. Vigolo
School of Chemical Engineering
University of Birmingham
Edgbaston, Birmingham B15 2TT, UK
D. Vigolo
School of Biomedical Engineering
The University of Sydney
Sydney, NSW 2006, Australia
D. Vella
Mathematical Institute
University of Oxford
Oxford OX2 6GG, UK

smart microgels have prospects for applications in this context and more generally as environmentally-responsive carriers for catalysis, drug release, and sensing.[12–18] Compared to bulk gels, spherical microgels have higher specific surface area and can thus promote more rapid exchange of substance between the microgels and environment;[19,20] spherical droplets can also highlight the liquid or liquid-like nature of the materials in another liquid.[5,6,21,22] Core–shell microgels present key advantages over homogeneous solid microgels, including the availability of both an outer and inner surface, and the ability to load the capsules with active ingredients. Such core–shell structures have gained increasing interest as nature-inspired phase-flexible constructs which can be exploited as biocompatible 3D hollow scaffolds to simulate organoids or mini tissues with cavity configuration, multi-release models, hierarchical bioreactors, tailor-made cells, or selective membranes to separate biomolecules statically and dynamically together with other progressive approaches.[11,23–26]

Developing core–shell microgels from proteins and their mechanical characterization is a key enabling technology in biomaterial mechanics research and regenerative medicine. Previous studies have showed the generation of core–shell non-protein microgels using two-step microfluidic techniques, 3D nested microcapillaries, or non-microfluidic methods.[27–31] Liquid–liquid phase separation (LLPS) studies are burgeoning because such phase separation phenomena are thought to be related to functional and aberrant biology as well as the processing of gel or liquid proteinaceous materials, especially at water–water interfaces.[5,6,9,21,32] Progress has also been made in aqueous two-phase systems that exhibit LLPS (Table S1, Supporting Information) as well as ECM or ECM-like systems with a high degree of biocompatibility introducing functional protein materials that are inhomogeneous.[5,6,9,16,19,33–39] However, complex manufacturing methods or harsh gelation conditions of protein-based gels can limit their applications, for instance, in regenerative medicine.[27,28,40–47] Generally regarded as safe (GRAS) materials by the FDA, such as gelatin and polyethylene glycol (PEG), have demonstrated significant application prospects at multiple scales for pharmaceuticals, cosmetics, and food products.[9,35,48–51] Recently, we have shown mild and versatile gelation regimes capable of producing physically- and enzymatically crosslinked gelatin microgels as collagen substitutes with radial density gradients, and we have further shown that gelatin microgels that can undergo a gel–sol transition could act as precursors of all-aqueous LLPS systems.[6,20] Developing all-aqueous emulsions from oil-free microgel precursors is a facile and simple approach that complements existing methods such as electrospray, 3D printing, glass capillary microfluidics, or hydrostatic pressure microfluidics.[6–8,37,52–55]

Here, we report robust, deformable, and smart gelatin microcapsules from GRAS materials which were processed via a one-step method in a 2D microfluidic device under mild gelation conditions and their potential usage scenarios in healthcare for cargo release and controlled degradability. Specifically, the minimization of surface energy in a liquid–liquid phase-separated system can drive the self assembly of the microcapsules from ECM-substituting protein, which makes the microcapsule production scalable, accessible, and controllable for medical applications with improved biocompatibility, bioactivity, and biomimicry. All-aqueous LLPS and multiphase-LLPS systems were generated with the gel–sol transition of microgel precursors in macromolecular crowders. This study demonstrates that microgels can both be the outcomes and the precursors of LLPS. LLPS of ECM proteins in aqueous environment can open up new application possibilities of advanced liquid material systems in biophysics, bioengineering, and biomedicine.

2. Results and Discussion

2.1. Formation of the Microgels

We fabricated microcapsules using a 2D four-inlet microfluidic device (**Figure 1**a; Figure S1, Movies S1 and S2, Supporting Information).[20] A gelatin/PEG liquid–liquid phase-separated system from GRAS materials was chosen (phase diagram shown in Figure S3, Supporting Information), in which the selected protein can be templated and crosslinked in a versatile and mild manner.[9,20,38,39] With microfluidic techniques, microcapsules with controllable shell thicknesses (E3–E5) and Janus microgels with controllable two-phase volume ratio (E1 and E2) were generated (Figure 1a–e). Clear interfaces between the PEG-rich and gelatin-rich phases meant these inhomogeneous microgels have sharp differences in composition (Figure 1b). 3D reconstruction of confocal imaging confirmed that each layer of the microcapsules had a closed gelatin layer, while Janus microgels did not (Figure 1f,g; Movies S3–S6, Supporting Information). Therefore, during demulsification, the PEG-rich phase remained encapsulated in microcapsules (sol–gel coexisting phase), but was washed off from the Janus microgels which turned into hole-shell microgels (gel phase only) (Figure 1b,f; Figure S4, Supporting Information).[56]

Despite the use of both PEG-in-gelatin or gelatin-in-PEG flow arrangements on the chip, we found that the microcapsules (E3–E5; E8–E10) always had gelatin shells and PEG cores (Figure 1a; Figure S4, Supporting Information). This finding suggests that it is the interfacial tensions of oil/gelatin, oil/PEG, and gelatin/PEG of the microdroplets that outweigh the geometrical constraints in droplet production (Figure S4, Supporting Information).[57] Previous studies have revealed an osmotic effect between two aqueous phase-separated phases;[8] thus, varying the volume fraction x_A can lead to a varying interfacial factor $(\gamma_A - \gamma_B)/\gamma_{AB}$ through water redistribution of the two aqueous phases in the microdroplets. The ultralow interfacial tension γ_{AB} characterizing the water/water interfaces would have larger impact on $(\gamma_A - \gamma_B)/\gamma_{AB}$, contributing to the Janus to core–shell transition (Figure 1h; Figure S5, Supporting Information).[8,37,58,59] The configurational transition in the present study (water/water/oil) complemented previous work on the varying inhomogeneity of double emulsions (water/oil/water).[60–62] Previous studies[61] showed that eccentric core–shell structures form because of the density difference of the

H. Yang
School of Mechanical Engineering
Hangzhou Dianzi University
Hangzhou 310018, P. R. China
A. P. M. Guttenplan
Department of Pharmacology
University of Cambridge
Cambridge CB2 1PD, UK

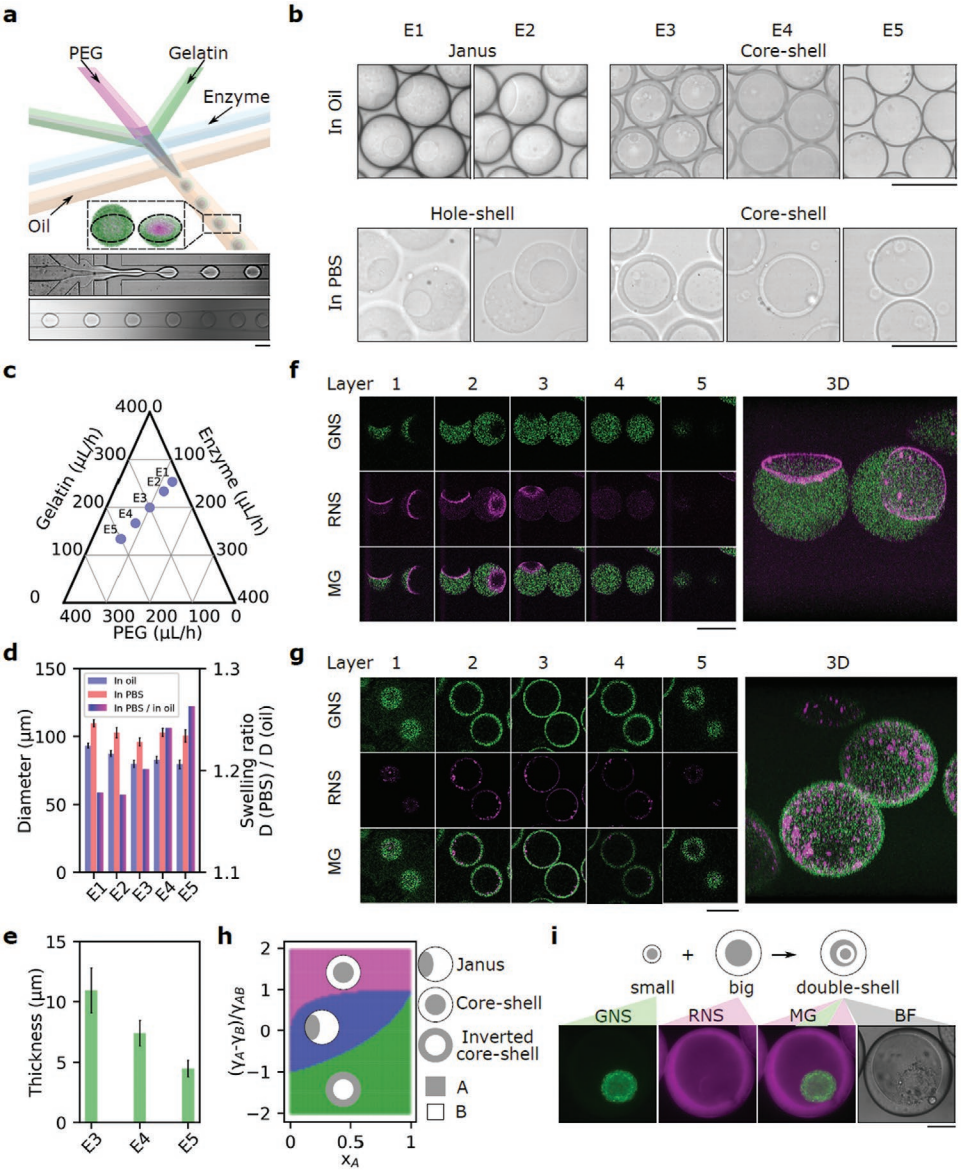

Figure 1. The formation of Janus microgels and core–shell microcapsules. a) The formation of microgels on a 2D microfluidic chip. A core–shell microgel and its cross section are shown in the schematic. Scale bar, 100 μm. b) Five different proportions of materials lead to Janus microgels or microcapsules (core–shell microgels). Janus microgels became hole-shell microgels after demulsification. No nanospheres were added in the microgels in (b). Scale bar, 100 μm. c) The flowrates of gelatin, PEG, and enzyme phases used to generate microgels shown in (b). d) Left, diameter of microgels in oil and demulsified in PBS, shown with the standard deviation in the bar chart. Each sample size of E1–E5 in oil and in PBS contains 100 realizations. Right, the swelling ratio of microgels, namely the ratio of diameter after to before demulsification. e) Thickness of the shells of microcapsules in (b,d) shown with the standard deviation. Each sample size of E3–E5 in PBS contains 100 realizations. f, g) Confocal images of hole-shell microgels (f) and microcapsules (g), layer 1–5 refers to five evenly spaced 2D layers of a 3D confocal imaging (Movies S3–S6, Supporting Information). Green nanospheres (GNSs) and red nanospheres (RNSs) were pre-mixed in the gelatin and PEG solutions, respectively. Scale bar, 100 μm. h) Phase diagram illustrating the minimum energy configurations of Janus, core–shell, and inverted core–shell microgels. Here, A and B are two immiscible aqueous solutions. x_A is the volume ratio of A solution in a droplet to that of the droplet. γ_A, γ_B, and γ_{AB} are interfacial tension coefficients at the interfaces of A solution/oil, B solution/oil, and A/B solution (Figure S5, Supporting Information). i) A double-shell microcapsule demonstrating a smaller microcapsule (GNSs in shell) encapsulated in a bigger microcapsule (RNSs in shell). Scale bar, 100 μm.

middle and outer phases combined with varying gelation time, which indicated that the middle/outer density mismatch could push the core off-center with respect to the shell.

We observed that both Janus microgels and core–shell microcapsules swelled when transferred from oil to aqueous phases; their diameters increased by ≈15–25% due to water uptake (Figure 1b,d). A larger size expansion was found in the microcapsules (E3–E5) relative to that of the hole-shell microgels (E1 and E2), a finding that highlighted the fact that the closed shells of the microcapsules could prevent the PEG leakage during demulsification (Figure 1b,d). The PEG-rich phase of hole-shell microgels dissolved during demulsification, and the swelling of hole-shell microgels depended solely on the gelatin-rich gel; in contrast, the PEG-rich cores of microcapsules stretched or

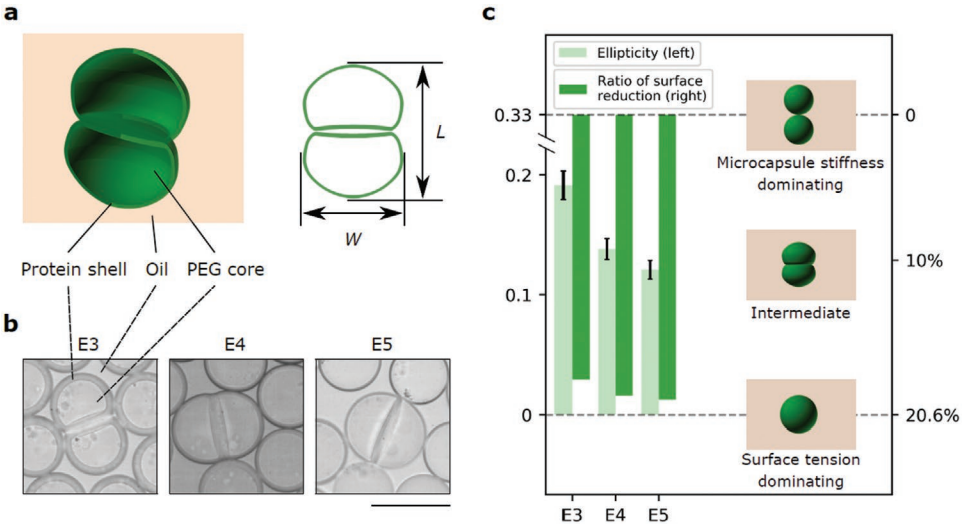

Figure 2. Analysis of the shapes of stressed microcapsules in oil. a,b) Schematic (a) and microscopy images (b) of two compressed microcapsules with varying thickness in oil. *L* and *W* respectively mean the length and the width of the structures (Figure S10, Supporting Information). Scale bar, 100 µm. c) The ellipticity (left *y*-axis) defined as $(L - W)/(L + W)$ of the structures in (a,b) shown with the standard error of the mean in the bar chart. Sample size of E3–E5 is respectively 33, 75, and 65. The ratio of reduction of the gel/oil surfaces (right *y*-axis) describes the decrease of gel/oil interfaces when two capsules in (a,b) get encapsulated into a single drop in oil. The *y*-axis position of the intermediate schematic was at the approximate position in the bar chart.

expanded the gelatin-rich shells during demulsification. We found that thinner-shell microcapsules (E5) swelled more than their thicker-shell counterparts (E3 and E4); interestingly, the diameter expansion ratio was empirically linear with the flow-rate ratio of gelatin to PEG solutions (Figure 1d; Figure S6, Supporting Information). One reason for this observed behavior is that thinner-shell microgels (E5) had larger PEG cores, which meant higher capacity for water absorption. The other reason is that the thinner-shell microcapsules (E5) were less mechanically robust to the swelling of the microcapsules, compared to thicker-shell microcapsules (E3 and E4). Demulsified microgels have the potential to be used for biological applications such as drug or cell-culture studies, exploiting the structural stability of physically- and enzymatically-crosslinked protein gels (Figure 1b).[20,50]

We next extended the approach to produce double-shell microcapsules by reinjecting the small microcapsules into a larger V-shaped flow-focusing device (Figure 1i; Figure S7, Supporting Information). These double-shell microcapsules can mimic complex natural hollow structures containing multi-compartmentalized structures, such as multi-layer ECM constructs, or could be used as multi-layer carriers for cell aggregates for artificial tissues or organs, and multi-layer reactors at small or big scales.[33]

2.2. Deformation of Microcapsules when Combining in Oil

We then probed the mechanical properties of the microcapsules using a microfluidic approach. To this effect, we focused on a minority population of droplets which had multiple cores consisting of two contacting microcapsules with compressed morphologies in a single oil drop (**Figure 2**a). We described the ellipticity of the two combining microcapsules in oil by the value $(L - W)/(L + W)$ that is related to the aspect ratio and can indicate the degree of their compression (Supporting Information). The encapsulation of two independent microcapsules in oil led to a reduction in the gel/oil interface area; this reduction was higher for thinner-shell microcapsules than for thicker-shell microcapsules, because more surface energy was converted into elastic strain energy of the thinner-shell capsules during their deformation (Figure S10c, Supporting Information). We found a larger compressive deformation of the thinner-shell microcapsules (E4 and E5) relative to thicker-shell microcapsules (E3) (Figure 2a–c). The ellipticity was a result of the balance between the stiffness of the two microcapsules and the hydrogel/oil interfacial properties; $(L - W)/(L + W)$ is expected to range from 0 to 1/3 (Figure 2c). Therefore, we qualitatively conclude that thicker-shell microcapsules (E3) were stiffer than thinner-shell microcapsules (E4 and E5) (Figure 2c). The encapsulation of the two microcapsules took place after the gelation of the protein shells, otherwise one bigger core–shell structure would have formed in oil (Figure 2a,b). In practice, we also found that the ellipticity value of the dual microcapsules increased after demulsification, suggesting the elastic deformation during their combination in oil or their water uptake during the demulsification into PBS.

2.3. Buckling of the Stress-Sensitive Microcapsules

We next probed the buckling of microcapsules by osmosis and by mechanical pressure. For soft biological systems, buckling can generate dramatic elastic deformations without significant changes in extensional strain. Buckling of surfaces and capsules has attracted attention for tunable surface functionalization, stretchable electronics, and biomechanics; a previous study showed the thermally-induced spontaneous buckling of polydispersed core–shell microgels with non-uniform thickness which were not made with microfluidic chips.[38,63–65] In

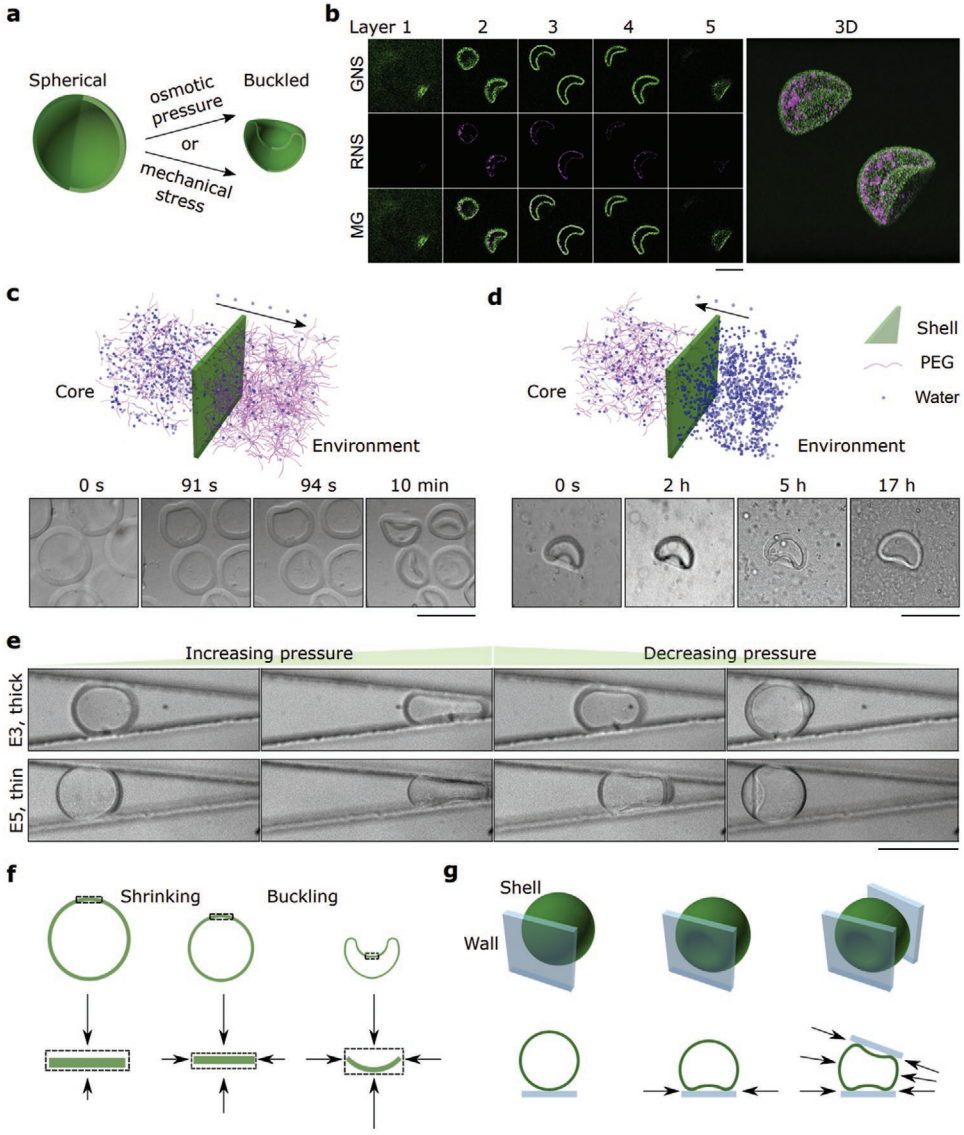

Figure 3. The stress-sensitive buckling of microcapsules. a) Schematic of cross section of a spherical microcapsule and a buckled microcapsule by osmotic pressure or mechanical pressure. b) Confocal imaging of a buckled microcapsule by osmotic pressure (Movies S7 and S8, Supporting Information). Scale bar, 100 µm. c,d) Time-lapse images of the dehydration (buckling, (c)) of microcapsules by osmotic pressure, and the rehydration (recovery, (d)) of a buckled microcapsule of (c) (Movies S9 and S10, Supporting Information). Scale bar, 100 µm. e) The bucking of a thick-shell or thin-shell microcapsule with increasing and decreasing oil pressure in a tapering microfluidic channel (Movies S11–S15, Supporting Information). Scale bar, 100 µm. A manuscript for this microfluidic device is being considered. f,g) Stress analysis in a buckled microcapsule by osmotic pressure (f) in (c), and by mechanical pressure (g) in (e).

our study, we explored buckling caused by two forms of environmental stimuli, osmotic pressure gradients, and direct mechanical stress.

2.3.1. Buckling by Osmosis

Osmosis-induced buckling was observed after a highly-concentrated PEG solution was added to the continuous PBS phase (**Figure 3**a–c; Movies S7–S9, Supporting Information). Confocal imaging showed that the protein-rich shells labeled by green nanospheres (GNSs) in each layer of *z*-stack images was smooth and closed with inner PEG-rich cores labeled by red nanospheres (RNSs), indicating that the buckling of these elastic microcapsules did not involve obvious fractures or bursts (Figure 3a,b). Buckling tended to start from the weakest or thinnest part of the microcapsules albeit their relatively uniform shell thickness (Figure 1b,d).[66] Buckling occurred rapidly within several minutes, but there was hardly any obvious recovery recorded during the 17-h time (Figure 3c,d; Movies S9 and S10, Supporting Information). During the buckling, dehydration and shrinkage of the cores took place, which involved the quick transfer of water molecules from the less-concentrated PEG cores to the highly-concentrated PEG continuous phase

(Figure 3c). As part of this dehydration, there was a decrease in the osmotic pressure difference between the PEG-rich core and the continuous PEG phase. The buckling ended when the stiffness of the protein shells was able to counterbalance the osmotic difference (Figure 3c). Buckling of core–shell microcapsules was not observed in low-concentration PEG solution (Figure S19, Supporting Information). Previous studies showed that shrinkage, flattening, and buckling were sequentially involved in 3D latex droplets;[67] and the shrinkage and a local depression at the drop surface led to both concave and convex interfaces on 2D droplets.[68] The buckling of microcapsules in the present study underwent similar processes (Figure 3c).[67,68] In contrast, the recovery process mainly resulted from the water uptake of the highly-concentrated PEG-rich cores. In this process, water molecules tended to overcome the water-PEG and PEG–PEG interactions and transferred from the continuous PEG phase to the PEG cores, and thus the PEG-rich cores swelled and became more diluted (Figure 3d). In practice, heating and stirring are usually needed to provide enough energy to promote the homogeneous dissolution or swelling of PEG in bulk solution. The water uptake of the dehydrated microcapsules was not an exact retraced course of the water loss of wetter microcapsules. These two processes can have different rates, as the degree of swelling of hydrogels depend on many factors such as network density, solvent nature, and polymer/solvent interactions.[69]

Before buckling, the osmotic pressure difference outside and inside a protein shell and the tensile stress in the protein shell are balanced, and therefore the microcapsules swelled during demulsification (Figures 1d and 3c). The addition of highly-concentrated PEG solution to the continuous phase triggered the deformation of the microcapsules in two steps: 1) shrinking of the shell and 2) inward buckling (Figure 3f). With the ongoing shrinking step, the tensile stress in the protein shells transformed into compressive stress with increasingly compact protein shells (Figure 3c,f). When the shell became nearly incompressible, then the inward buckling step began at the weakest or thinnest part of the shells, including flattening and inward concaving (Figure 3c,f).[70,71] The deflection, or the indentation, of the shell was perpendicular to the concentrated compressive stresses, further increased by the osmotic pressure (Figure 3f). The buckling caused a concave surface and a convex surface of the microcapsule, and the work done by osmotic pressure was transformed into the strain energy stored in the microcapsule. Buckling thicker-shell microcapsules (E3) would need more energy than thinner-shell microcapsules (E4 and E5); it is well known that the energetic cost of bending a thin sheet (thickness, t) scales with t^3.[10] Bending energy and elastic energy are closely related to the conformations of the buckled invagination, and the critical external pressure required to trigger the buckling scales with t^2/R^2 (R, capsule radius; see Supporting Information and Figure S11, Supporting Information, for a justification of this scaling law).[10,70,71] With increasing loss of the capsule volume, the bucked zone can even experience a transition from an axisymmetric dimple (primary buckling) to asymmetrical wrinkles (secondary buckling).[72,73] Capsules with a lower bending stiffness and with a larger volume loss are more likely to develop secondary buckling.[61,73]

2.3.2. Buckling by Mechanical Pressure

We next explored buckling caused by mechanical pressure in a microfluidic mechanical testing device.[74] In this geometry, the oil pressure drop pushed a microcapsule into the narrow part of a tapering channel where deformation of the microcapsule occurred (Figure 3a,e). When a microcapsule made contact with the PDMS walls, the shell first became flattened; further compressing of the microcapsules led to increasing contact area between the shell and the PDMS walls, and the accumulated compressive stress then buckled the microcapsules (Figure 3g; Movies S11–S15, Supporting Information). The buckling induced by the mechanical pressure was a result of the compressive stresses (Figure 3e,g; Figure S12, Supporting Information). After the unloading of the oil pressure, the microcapsules remained buckled, which indicated that the water drop outside the shell in the oil could not be immediately reabsorbed by the protein-rich or PEG-rich phases as previously discussed in this present study (Figure 3d). Therefore, the buckling of the microcapsules was relatively permanent (Figure 3c,e). The method presented in this study therefore offers a new route for the creation of passive (mechanical force assisting) semipermeable membranes, as well as applications in lock-and-key structures for bodies and hinges or joints of biocompatible and bioactive soft robots.[75,76]

Recent studies show that the oil/surfactant composition can affect the morphology of water/oil droplets in contact with each other, and there is a tendency to form planar gel/gel interfaces when solid microgels contact in oil.[33,77] However, when two microcapsules come into contact in a continuous oil phase (Figure 2b; Figure S10a, Supporting Information), the shell/core interfaces near the shell/shell contact surfaces were slightly curved, indicating deformation of the shells of the microcapsules at the shell/shell interfaces. It is therefore feasible to visualize the deformation of the microcapsules. This deformation by interfacial tension (Figure 2b; Figure S10a, Supporting Information) is less obvious than that by osmosis or mechanical force (Figure 3c,e). Since buckling decreases the core volume, it can be inferred that water must be transported out through the shell (Figure 2a,b; Figure S10b,c, Supporting Information).

In previous studies, the inward buckling of core–shell microgels with gradually-varied shell thickness was accompanied by triangular or other polygonal indentations;[61] thin shells or layers had multiple and periodic wrinkles during buckling.[10,78] This buckling is driven by the stress induced by buckling, which can be inferred directly from changes in the shell's Gaussian curvature (Figure S13, Supporting Information).[10] In contrast, the buckling morphologies we observe remain axisymmetric and smooth in this present study (Figure 3). One reason that we do not observe polygonal instabilities might be the relatively uniform shell thickness (Figures 1e and 3); the other possible reason is that the microcapsules are not as thin as those in other studies, and the shell elasticity plays a key role in maintaining the morphological smoothness during buckling (Figure 1e).[10,70–73] The key parameter that controls this is the Föppl-von-Kármán-number $\gamma_{FvK} = 12R^2(1-\nu^2)/t^2$, where R, ν, and t are the outer radius, Poisson ratio, and thickness of the capsule, respectively.[72] Previous theoretical work showed that if

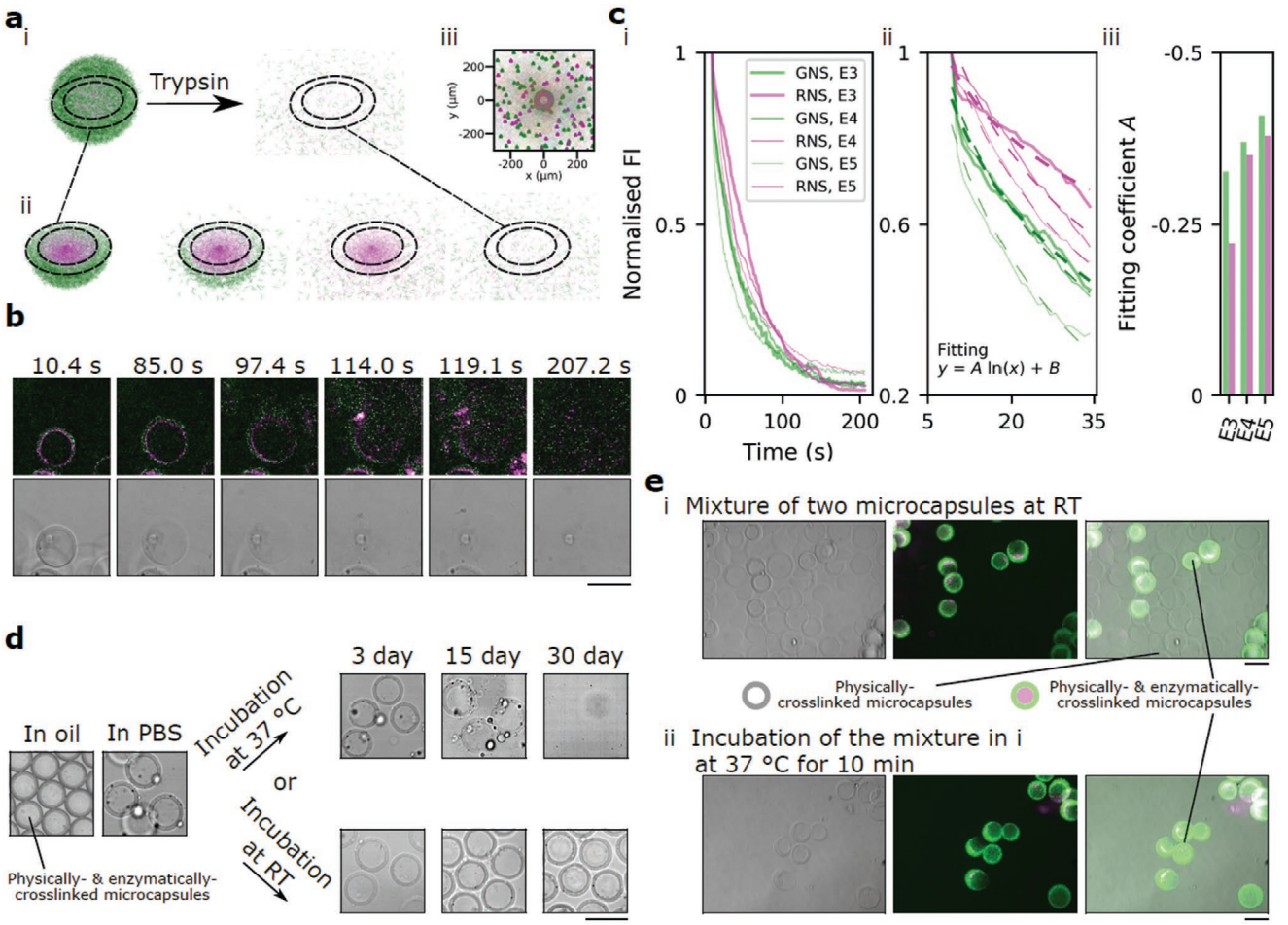

Figure 4. Sequential dual release of nanospheres from the microcapsules and the thermostability of the microcapsules. a) Schematics of the sequentially dual release of nanospheres of microcapsules. A full microcapsule (i), the cross section of the microcapsule, the gelatin/PBS and gelatin/PEG boundaries were shown by dashed circles (ii), simulation (Figure S15, Supporting Information) of the nanosphere positions and moving paths following Brownian motion, before the shell dissolution of a microcapsule (GNSs, green circles; RNSs, red circles) and after the complete dissolution of the microcapsule (GNSs, green triangles; RNSs, red triangles) (iii). b) Time-lapsed images (2D confocal imaging) of the release of GNSs from shells and the RNSs from the cores of the microcapsules with medium thickness (E4) during the enzymatic digestion. Scale bar, 100 μm. c) Sequential dual release of GNSs from shells and RNSs from cores of microcapsules with varying shell thickness. Standard deviation and more details can be found in Figure S14, Supporting Information and the sample size of E3–E5 is respectively 126, 107, 108 (i). The beginning of the release curves in (i) was fitted to $y = A\ln(x) + B$ (ii). Coefficient A was shown in bar chart. FI, fluorescence intensity (iii). d) Thermostability of physically-crosslinked and enzymatically-crosslinked microcapsules (E3). Scale bar, 100 μm. e) The mixture of the two kinds of microcapsules was kept at RT (i). Then the physically-crosslinked microcapsules dissolved after the mixture was incubated at 37 °C for 10 min. Scale bar, 100 μm (ii).

$\gamma_{FvK} < \gamma^{c}_{FvK} \approx 10^4$, then only the primary buckling is observed, not the secondary buckling event.[61,72,73] Here, $t \approx 5$ μm, $R \approx 50$ μm (Figure 1d,e), so that $\gamma_{FvK} \approx 10^3 \lesssim \gamma^{c}_{FvK}$, the microcapsules are closer in aspect ratio t/R to a tennis ball, which maintains a smooth invagination upon buckling.[79]

2.4. Degradable Microcapsules as Drug Release Models

We explored the potential of the capsules for multi-step release of multiple cargo species. Following enzymatic digestion of protein shells, we observed the sequential release of GNSs from the shells and RNSs from the cores (**Figure 4**b,c). In addition, RNSs in thinner-shell capsules (E5) had a faster release than those in thicker-shell capsules (E3 and E4), because the degradation of thinner-shell capsules took place in a shorter time (Figure 4c; Figure S14, Supporting Information). ECM-based protein capsules could be digested by collagenases, trypsin, matrix metallopeptidases, or elastases in mammals.[16,80] Therefore, the principle of the sequential dual release also holds potential for personalized or nanoparticle-based medicine in vivo, particularly when a time-sensitive therapy requires the delivery of two drugs to target disease focuses.

Following the enzyme-induced release, we next explored temperature-induced depolymerization of the protein shells; previous studies demonstrated rupture of the synthetic-polymer shells, for example, induced by osmotic pressure or by an

nonlinear interfacial electrokinetic stress.[60,81] Gelatin can be crosslinked enzymatically as a result of the covalent bond connecting lysine and glutamine residues with the presence of transglutaminase, or crosslinked physically because of the noncovalent interactions such as Van der Waals' forces, hydrogen bonding, hydrophobic interaction, and electrostatic interaction.[20] With transglutaminase, the gelatin shells underwent first physical crosslinking and then enzymatic crosslinking, which contributed to the robust networks of peptide chains of gelatin and thus improved the thermostability of the microcapsules at 37 °C (Figure 4d,e). The microcapsules fabricated through physical and enzymatic crosslinking were thermostable at 37 °C for more than 2 weeks, and thermostable at room temperature (RT) for more than 1 month (Figure 4d). One reason of this difference is that the crosslinked triple helices were more likely to untwist at 37 °C, leading to a larger population of random coils and the gradual weakening of the hydrogels. The other explanation is that degradation was accelerated by the action of microorganism at 37 °C (Figure 4d). In contrast, we also made physically-crosslinked microcapsules without transglutaminase (Figure 4e and Figure S16, Supporting Information). After demulsification, these physically-crosslinked microcapsules remained thermostable in PBS at RT, but dissolved quickly (less than 10 min) in PBS at 37 °C (Figure 4e). The gelation through only physical crosslinking was weak and reversible. A possible application taking advantage of both these crosslinking approaches could be a thermosensitive and implantable medicine (Figure 4e). This can be used for personalized medicine, nanoparticle-based therapies, and artificial tissue scaffolds as asynchronous drug carriers for short-term and long-term releases in vivo or in vitro.[82,83]

2.5. Formation of All-Aqueous LLPS or Multiphase LLPS Systems by Reversing the Crosslinking

Our recent study demonstrated the formation of all-aqueous LLPS systems with microgel precursors in aqueous crowded environment.[6] This present study moved another step forward for the formation of LLPS (two-phase) and multiphase-LLPS systems by the gel–sol transition of physically crosslinked microgel precursors in PEG crowder (**Figure 5**). Hole-shell (Janus) microgels evolved into spherical droplets in PEG solution when heated to 37 °C, and the coalescence of droplets in close proximity was also observed (Figure 5a). Buckled core–shell microgels in PEG solution at RT notably converted to spherical core–shell droplets when heated to 37 °C (Figure 5b; Figure S17, Supporting Information). The coalescence of such buckled core–shell droplets was also observed; the shells coalesced because of wetting, before the fusion of cores (Figure 5b). Enzymatically crosslinked Janus or buckled core–shell microgels, however, remained intact morphologically when heated to 37 °C, which further highlighted that enzymatically crosslinked gelatin gel would not undergo thermo-induced gel–sol transition (Figure S18, Supporting Information). The formation of LLPS (two-phase, Figure 5a) or multiphase-LLPS (Figure 5b) systems from microgel precursors provided a simple and facile approach to generating all-aqueous emulsion without direct on-chip generation that usually required additional setups.[6–8,37,52–55] Previously, the fusion of core–shell structures was reported in water-oil-water double emulsion or RNA-protein hollow condensates;[84,85] this present study extends the fusion phenomena to crowder-protein-crowder all-aqueous interfaces and has the potential to inspire the explanation of the fusion of hollow-like structures or multiphase condensates from other materials (Figure 5b). On the one hand, the formation of Janus and core–shell microgels (Figure 1) was achieved by gelatin/PEG LLPS and by the sol–gel transition (gelation) of gelatin. On the other hand, these microgels can be intriguingly facilitated to fabricate all-aqueous LLPS or multiphase LLPS systems by the gel–sol transition (reversing crosslinking) of gelatin (Figure 5). Our recent study demonstrated that LLPS from solid gelatin microgel precursors in PEG solution of relatively high PEG concentration;[6] similarly, in this present study, multiphase LLPS from core–shell microgel precursors took place in PEG solution of relatively high concentration (Figure S19, Supporting Information). Higher concentration of macromolecular crowding has higher depletion force and excluded volume effect that supports LLPS or multiphase LLPS.[6,7,9,21,86]

3. Conclusions

In summary, we have demonstrated a route toward the fabrication of monodisperse core–shell gelatin microcapsules with controllable and varying shell thickness. The spontaneous formation of the microcapsules exploited aqueous LLPS. Physical and enzymatic crosslinking approaches further stabilized the protein shells. The degradable microcapsules are promising as implants or nanoparticle-based therapies for sequential release or temperature-sensitive implants. Interfacial tension, osmosis, and mechanical pressure were utilized to probe the deformation of these microcapsules. Through gel–sol transition, microgels functioned as precursors for the formation of all-aqueous liquid–liquid phase-separated systems that were two-phase or multiphase. Thus, the microgels were both the outcomes and precursors of LLPS in this study. Taken together, our results suggested that core–shell protein microcapsules are a class of materials with potential applications in areas that are influenced by material micromechanics and phase versatility.

4. Experimental Section

Materials Preparation: PEG solution (30 mg mL^{-1}) was made by dissolving PEG powder (molecular weight 300 000; Sigma-Aldrich Co. Ltd., MO, US; product of USA) in phosphate buffered saline (PBS; Oxoid Ltd, Hampshire, UK) at 50 °C with magnetic stirring for 5 h. Gelatin solution (75 mg mL^{-1}) was made by dissolving gelatin powder (Sigma-Aldrich Co. Ltd., MO, US; product of Germany) in PBS at 50 °C with magnetic stirring for 2 h. Enzyme solution, that is, transglutaminase solution (50 mg mL^{-1}), was made by dissolving transglutaminase powder (Special Ingredients Ltd., Chesterfield, UK; product of Spain) in PBS at RT for 2 h, and the solution was then filtrated with a 0.22 µm filter. Gelatin solution and enzyme solution were then kept at 4 °C and used within 1 week. For nanoparticle encapsulation, GNSs (200 nm, 1% solids, Fluoro-Max, Thermo Scientific, CA, US) were pre-mixed in the gelatin solution (1/100) v/v, and RNSs (100 nm, 1% solids, Fluoro-Max, Thermo Scientific, CA, US) were pre-mixed in PEG solution (1/100)

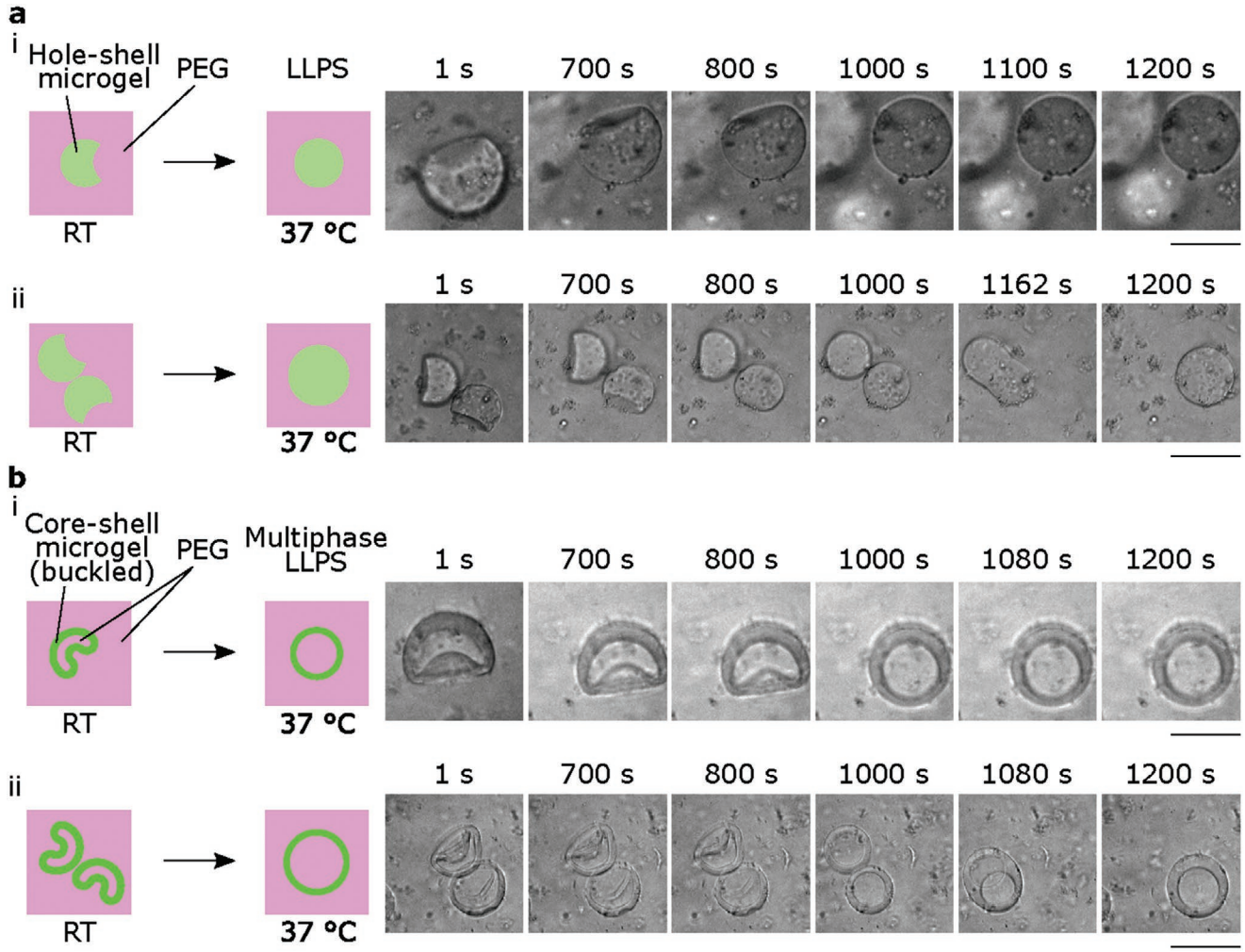

Figure 5. All-aqueous LLPS and multiphase LLPS from the gel–sol transition of physically crosslinked microgels in a macromolecular crowder. a) All-aqueous LLPS (two-phase). Gel–sol transition of a hole-shell (Janus) microgel in PEG solution (Movie S16, Supporting Information). Scale bar, 50 µm (i). Coalescence of two liquefied hole-shell microgels in PEG solution (Movie S17, Supporting Information). Scale bar, 100 µm (ii). b) All-aqueous multiphase LLPS. Gel–sol transition of a buckled core-shell microgel in PEG solution (Movie S18 and Figure S17, Supporting Information). Scale bar, 50 µm (i). Coalescence of two liquefied core–shell microgels in PEG solution (Movie S19, Supporting Information). Scale bar, 100 µm (ii). Finite element simulation can be found in Figure S20, Supporting Information.

v/v. Fluorosurfactant (2%) w/w (RAN biotechnologies, MA, US) was dissolved in Fluorinert (FC-40; TM, Reg; Fluorochem, Hadfield, UK) as the continuous oil phase.

Microgel Formation: Microfluidic devices were fabricated by soft-lithography techniques as previously reported.[87] A temperature-controlled microfluidic setup was used as previously reported.[20] Flow-focusing V-shaped microfluidic chips were used to make physically and enzymatically crosslinked gelatin microgels. 1) To form physically-crosslinked and enzymatically-crosslinked gelatin microgels, PEG solution, gelatin solution, enzyme solution, and continuous oil phase were loaded in four separate syringes with polythene tubings. The tubing containing gelatin phase was fixed on a hot plate at 37 °C. The flowrates of these liquids were controlled by a neMESYS pump system (CETONI GmbH, Korbussen, Germany). The inlet positions of the PEG solution and enzyme solution were also switched for different experiment geometries. The microdroplets were formed at the flow-focusing junctions of the microfluidic chips at 37 °C, and were then collected and incubated in Eppendorf tubes at room temperature (RT) overnight. The microgels were then demulsified with 10% 1H,1H,2H,2H-perfluoro-1-octanol (Sigma-Aldrich Co. Ltd., MO, US) and finally rinsed in PBS.[19] 2) To form physically-crosslinked gelatin microgels, PEG solution, gelatin solution, PBS, and continuous oil phase were loaded in four separate syringes with polythene tubings. Similarly, the microdroplets were formed at the flow-focusing junctions of the microfluidic chips at 37 °C, and were then collected and incubated in Eppendorf tubes at RT overnight. The microgels were then demulsified with 10% 1H,1H,2H,2H-perfluoro-1-octanol at RT or lower temperature. 3) The calculation of Janus to core–shell transition could be found in Supporting Information.

Optical Microscopy: 1) The bright-field images of the formation of microdroplets were taken with a high-speed camera (MotionBLITZ EoSens Mini1-1 MC1370, Mikrotron, Unterschleissheim, Germany) on a microscope (Oberver.A1, Axio, Zeiss, Oberkochen, Germany). The dark-field fluorescent images of the microgels were taken with a CCD camera (CoolSNAP MYO, Photometrics, AZ, US) on the abovementioned microscope; for the GNSs and RNSs, a 49001 filter (excitation wavelength 426–446 nm, emission wavelength 460–500 nm) and a 49004 filter (excitation wavelength 532–557 nm and emission wavelength 570–640 nm) were respectively used with a compact light source (HXP 120 V, Leistungselektronik Jena GmbH, Jena, Germany). 2)

Confocal images were taken on a microscope (Leica TCS SP5, Germany) for GNSs (excitation wavelength 468 nm, emission wavelength 508 nm) and RNSs (excitation wavelength 542 nm and emission wavelength 612 nm). Data were analyzed with Python and ImageJ.

Phase Diagram: Gelatin solution (0–100 mg mL^{-1} stepwise) and PEG solution (0–60 mg mL^{-1} stepwise) were mixed v/v (1:1) at 37 °C on a vortex mixer (Fisherbrand) at 2000 rpm for 20 s. Brightfield images of miscibility of the two solutions were immediately taken. Obvious water–water emulsion was considered two-phase.

Microcapsules Encapsulated in a Single Oil Drop: Microcapsules in oil were transferred from the Eppendorf tubes to glass slides. A minority population of microcapsules had spontaneously combined, resulting in the forms of two or more microcapsules in a single oil drop. Brightfield microscopy images were taken.

Buckling Studies: 1) Buckling through osmotic pressure. A highly-concentrated PEG solution (60 mg mL^{-1}) was added to the demulsified microcapsule solution v/v (3/1) to cause the dehydration of microcapsules. Then, this PEG solution was removed, and PBS was added to the microcapsules to study the rehydration of microcapsules. 2) Buckling through mechanical forces. Microcapsules in oil were squeezed into a microfluidic device (manuscript being considered);[74] additional oil was injected into the bypass channel of the device at different flowrates. Images were were taken with the abovementioned CCD camera or high-speed camera on the abovementioned microscope.

Microcapsule Dissolution: 1) Trypsin (concentration 0.25%) (Life Technologies Ltd., Paisley, UK) was added to the physically- and enzymatically-crosslinked microcapsules in PBS 1/1 (v/v) in a 96-well UV-transparent half area plate (Corning Incorporated, ME, US); and the dark-field fluorescent time-lapse images for GNSs and RNSs were taken with the abovementioned CCD camera and microscope with the abovementioned 49001 filter and 49004 filter. 2D confocal imaging was also performed on the abovementioned confocal microscope. 2) Microcapsules in PBS were incubated at 37 °C, and then their existence was checked on a microscope to determine their thermal robustness or stability with time.

Formation of All-Aqueous LLPS Systems and Multiphase-LLPS Systems from Microgel Precursors: 1) All-aqueous LLPS system. The Janus (hole-shell) microgel suspension was mixed with 6% (i.e., 60 mg mL^{-1}) PEG solution v/v, (1/10) at RT. Such mixture was heated to 37 °C to form an LLPS system. 2) All-aqueous multiphase-LLPS system. The core–shell microgel suspension was mixed with 6% PEG solution v/v, (1/10) at RT. Such mixture was heated to 37 °C to form a multiphase-LLPS system. Imaging was conducted at 37 °C in a thermostatic chamber.

Supporting Information

Supporting Information is available from the Wiley Online Library or from the author.

Acknowledgements

The research leading to these results has received funding from the Cambridge Trust (Y.X. and B.L.), the Jardine Foundation (Y.X.), Trinity College Cambridge (Y.X.), Peterhouse College Cambridge (T.C.T.M.), the Swiss National Science Foundation (T.C.T.M.), the Engineering and Physical Sciences Research Council (K.L.S.), the Schmidt Science Fellowship program in partnership with the Rhodes Trust (K.L.S.), St John's College Cambridge (K.L.S.), China Scholarship Council (H.Z. and B.L.), EPSRC Cambridge NanoDTC (EP/037221/1; A.P.M.G.), the Newman Foundation (T.P.J.K.), the Wellcome Trust (T.P.J.K.), and the European Research Council under the European Union's Seventh Framework Programme (FP7/2007-2013) through the ERC grant PhysProt (agreement no. 337969; T.P.J.K.).

Conflict of Interest

The authors declare no conflict of interest.

Author Contributions

Y.X. and T.P.J.K. conceived and designed the experiments. Y.X. developed the microgels, performed the experiments, and analyzed the data. Y.S. advised on the experiments. T.C.T.M. and Y.X. developed the surface energy calculation. Y.X. and K.N.B. performed the confocal microscopy experiments. Y.X. and Q.P. studied the buckling process. D.V. gave useful advice on the buckling studies. A.P.M.G. and K.L.S. originally designed the mechanical testing microfluidic device which was modified by Y.S., Y.L., and Y.X. in Figure 3e. B.L. and D.K. assisted at the imaging for Figure 5. H.Y. performed the finite element simulation. Y.X. wrote the paper and all authors commented on the paper.

Data Availability Statement

The data that support the findings of this study are available from the corresponding author upon reasonable request.

Keywords

all-aqueous emulsions, buckling, core–shell microgels, extracellular matrix, Janus microgels, liquid–liquid phase separation, protein microgels

Received: June 25, 2021
Published online:

[1] D. E. Discher, D. J. Mooney, P. W. Zandstra, *Science* **2009**, *324*, 1673.
[2] L. Sapir, S. Tzlil, *Semin. Cell Dev. Biol.* **2017**, *71*, 99.
[3] J. L. Puetzer, T. Ma, I. Sallent, A. Gelmi, M. M. Stevens, *Biomaterials* **2021**, *269*, 120527.
[4] T. J. Welsh, Y. Shen, A. Levin, T. P. J. Knowles, *Cell* **2018**, *175*, 1457.
[5] Y. Shen, F. S. Ruggeri, D. Vigolo, A. Kamada, S. Qamar, A. Levin, C. Iserman, S. Alberti, P. St George-Hyslop, T. P. J. Knowles, *Nat. Nanotechnol.* **2020**, *15*, 841.
[6] Y. Xu, R. Qi, H. Zhu, B. Li, Y. Shen, G. Krainer, D. Klenerman, T. P. J. Knowles, *Adv. Mater.* **2021**, 2008670.
[7] Q. Ma, Y. Song, W. Sun, J. Cao, H. Yuan, X. Wang, Y. Sun, H. C. Shum, *Adv. Sci.* **2020**, *7*, 1903359.
[8] Y. Song, T. C. T. Michaels, Q. Ma, Z. Liu, H. Yuan, S. Takayama, T. P. J. Knowles, H. C. Shum, *Nat. Commun.* **2018**, *9*, 2110.
[9] G.-L. Ying, N. Jiang, S. Maharjan, Y.-X. Yin, R.-R. Chai, X. Cao, J.-Z. Yang, A. K. Miri, S. Hassan, Y. S. Zhang, *Adv. Mater.* **2018**, *30*, 1805460.
[10] D. Vella, *Nat. Rev. Phys.* **2019**, *1*, 425.
[11] C. Bertulli, M. Gerigk, N. Piano, Y. Liu, D. Zhang, T. Müller, T. J. Knowles, Y. Y. S. Huang, *Scientific reports* **2018**, *8*, 12480.
[12] S. Seiffert, *Angew. Chem., Int. Ed.* **2013**, *52*, 11462.
[13] S. Seiffert, *ChemPhysChem* **2013**, *14*, 295.
[14] C. Li, L. Ouyang, J. P. Armstrong, M. M. Stevens, *Trends Biotechnol.* **2021**, *39*, 150.
[15] H. Liu, Y. Wang, K. Cui, Y. Guo, X. Zhang, J. Qin, *Adv. Mater.* **2019**, *31*, 1902042.
[16] A. K. Gaharwar, I. Singh, A. Khademhosseini, *Nat. Rev. Mater.* **2020**, *5*, 686.

[17] U. Kauscher, M. N. Holme, M. Björnmalm, M. M. Stevens, *Adv. Drug Deliv. Rev.* **2019**, *138*, 259.
[18] L. Zwi-Dantsis, C. W. Winter, U. Kauscher, A. Ferrini, B. Wang, T. E. Whittaker, S. R. Hood, C. M. Terracciano, M. M. Stevens, *Nanoscale* **2020**, *12*, 19844.
[19] A. S. Mao, J.-W. Shin, S. Utech, H. Wang, O. Uzun, W. Li, M. Cooper, Y. Hu, L. Zhang, D. A. Weitz, D. J. Mooney, *Nat. Mater.* **2017**, *16*, 236.
[20] Y. Xu, R. P. B. Jacquat, Y. Shen, D. Vigolo, D. Morse, S. Zhang, T. P. J. Knowles, *Small* **2020**, *16*, 2000432.
[21] C. Yuan, M. Yang, X. Ren, Q. Zou, X. Yan, *Angew. Chem., Int. Ed.* **2020**, *59*, 17456.
[22] L. Jawerth, E. Fischer-Friedrich, S. Saha, J. Wang, T. Franzmann, X. Zhang, J. Sachweh, M. Ruer, M. Ijavi, S. Saha, J. Mahamid, A. A. Hyman, F. Jülicher, *Science* **2020**, *370*, 1317.
[23] W. Wang, K. Ouaras, A. L. Rutz, X. Li, M. Gerigk, T. E. Naegele, G. G. Malliaras, Y. Y. S. Huang, *Sci. Adv.* **2020**, *6*, eaba0931.
[24] L. Zhou, A. C. Wolfes, Y. Li, D. C. Chan, H. Ko, F. G. Szele, H. Bayley, *Adv. Mater.* **2020**, *32*, 2002183.
[25] X. Liu, J. Tao, J. Liu, X. Xu, J. Zhang, Y. Huang, Y. Chen, J. Zhang, D. Y. B. Deng, M. Gou, Y. Wei, *ACS Appl. Mater. Interfaces.* **2019**, *11*, 12209.
[26] S. Nam, D. Mooney, *Chem. Rev.* **2021**, https://doi.org/10.1021/acs.chemrev.0c00798
[27] S. Seiffert, J. Thiele, A. R. Abate, D. A. Weitz, *J. Am. Chem. Soc.* **2010**, *132*, 6606.
[28] M. Seuss, W. Schmolke, A. Drechsler, A. Fery, S. Seiffert, *ACS Appl. Mater. Interfaces* **2016**, *8*, 16317.
[29] K. Zhu, Y. Yu, Y. Cheng, C. Tian, G. Zhao, Y. Zhao, *ACS Appl. Mater. Interfaces* **2019**, *11*, 4826.
[30] D. B. Shenoy, G. B. Sukhorukov, *Macromol. Biosci.* **2005**, *5*, 451.
[31] J. Dubbert, K. Nothdurft, M. Karg, W. Richtering, *Macromol. Rapid Commun.* **2015**, *36*, 159.
[32] C. P. Brangwynne, C. R. Eckmann, D. S. Courson, A. Rybarska, C. Hoege, J. Gharakhani, F. Jülicher, A. A. Hyman, *Science* **2009**, *324*, 1729.
[33] F. G. Downs, D. J. Lunn, M. J. Booth, J. B. Sauer, W. J. Ramsay, R. G. Klemperer, C. J. Hawker, H. Bayley, *Nat. Chem.* **2020**, *12*, 363.
[34] K. Tsumoto, K. Yoshikawa, *MRS Adv.* **2017**, *2*, 2407.
[35] G. Luo, Y. Yu, Y. Yuan, X. Chen, Z. Liu, T. Kong, *Adv. Mater.* **2019**, *31*, 1904631.
[36] U. Shimanovich, Y. Song, J. Brujic, H. C. Shum, T. P. J. Knowles, *Macromol. Biosci.* **2015**, *15*, 501.
[37] Y. Song, U. Shimanovich, T. C. T. Michaels, Q. Ma, J. Li, T. P. J. Knowles, H. C. Shum, *Nat. Commun.* **2016**, *7*, 12934.
[38] K. Koyanagi, K. Kudo, M. Yanagisawa, *Langmuir* **2019**, *35*, 2283.
[39] M. Yanagisawa, S. Nigorikawa, T. Sakaue, K. Fujiwara, M. Tokita, *Proc. Natl. Acad. Sci. USA* **2014**, *111*, 15894.
[40] M. Michelon, Y. Huang, L. G. de la Torre, D. A. Weitz, R. L. Cunha, *Chem. Eng. J.* **2019**, *366*, 27.
[41] M. L. Eggersdorfer, W. Zheng, S. Nawar, C. Mercandetti, A. Ofner, I. Leibacher, S. Koehler, D. A. Weitz, *Lab Chip* **2017**, *17*, 936.
[42] Q. Chen, S. Utech, D. Chen, R. Prodanovic, J.-M. Lin, D. A. Weitz, *Lab Chip* **2016**, *16*, 1346.
[43] S. Deshpande, Y. Caspi, A. E. C. Meijering, C. Dekker, *Nat. Commun.* **2016**, *7*, 10447.
[44] M. Windbergs, Y. Zhao, J. Heyman, D. A. Weitz, *J. Am. Chem. Soc.* **2013**, *135*, 7933.
[45] H. C. Shum, D. Lee, I. Yoon, T. Kodger, D. A. Weitz, *Langmuir* **2008**, *24*, 7651.
[46] S. Liang, J. Li, Q. Xu, J. Man, H. Chen, *Small* **2018**, *14*, 1800613.
[47] H. Zhu, S. Nawar, J. G. Werner, J. Liu, G. Huang, Y. Mei, D. A. Weitz, A. A. Solovev, *J. Phys. Condens. Matter* **2019**, *31*, 214004.
[48] R. M. Hathout, M. K. Omran, *Pharm. Dev. Technol.* **2016**, *21*, 379.
[49] Q. Yang, S. K. Lai, *Wiley Interdiscip. Rev. Nanomed. Nanobiotechnol.* **2015**, *7*, 655.
[50] C. W. Yung, L. Q. Wu, J. A. Tullman, G. F. Payne, W. E. Bentley, T. A. Barbari, *J. Biomed. Mater. Res. A* **2007**, *83*, 1039.
[51] H. Wang, H. Liu, H. Liu, W. Su, W. Chen, J. Qin, *Adv. Mater. Technol.* **2019**, *4*, 1800632.
[52] M. Jeyhani, R. Thevakumaran, N. Abbasi, D. K. Hwang, S. S. H. Tsai, *Small* **2020**, *16*, 1906565.
[53] B.-U. Moon, N. Abbasi, S. G. Jones, D. K. Hwang, S. S. H. Tsai, *Anal. Chem.* **2016**, *88*, 3982.
[54] A. Sauret, H. Cheung Shum, *Appl. Phys. Lett.* **2012**, *100*, 154106.
[55] Y. Song, Y. K. Chan, Q. Ma, Z. Liu, H. C. Shum, *ACS Appl. Mater. Interfaces* **2015**, *7*, 13925.
[56] W. Wang, M.-J. Zhang, R. Xie, X.-J. Ju, C. Yang, C.-L. Mou, D. A. Weitz, L.-Y. Chu, *Angew. Chem., Int. Ed.* **2013**, *52*, 8084.
[57] G. Tubio, B. Nerli, G. Picó, *J. Chromatogr. B* **2004**, *799*, 293.
[58] D. Forciniti, C. K. Hall, M. R. Kula, *J. Biotechnol.* **1990**, *16*, 279.
[59] Y. Liu, R. Lipowsky, R. Dimova, *Langmuir* **2012**, *28*, 3831.
[60] W. Zhang, L. Qu, H. Pei, Z. Qin, J. Didier, Z. Wu, F. Bobe, D. E. Ingber, D. A. Weitz, *Small* **2019**, *15*, 1903087.
[61] S. S. Datta, S.-H. Kim, J. Paulose, A. Abbaspourrad, D. R. Nelson, D. A. Weitz, *Phys. Rev. Lett.* **2012**, *109*, 134302.
[62] A. S. Utada, E. Lorenceau, D. R. Link, P. D. Kaplan, H. A. Stone, D. A. Weitz, *Science* **2005**, *308*, 537.
[63] L. Stein-Montalvo, P. Costa, M. Pezzulla, D. P. Holmes, *Soft Matter* **2019**, *15*, 1215.
[64] T. C. T. Michaels, R. Kusters, A. J. Dear, C. Storm, J. C. Weaver, L. Mahadevan, *Proc. Math. Phys. Eng. Sci.* **2019**, *475*, 20190370.
[65] P. M. Reis, *J. Appl. Mech.* **2015**, *82*, 111001.
[66] S. S. Datta, A. Abbaspourrad, E. Amstad, J. Fan, S.-H. Kim, M. Romanowsky, H. C. Shum, B. Sun, A. S. Utada, M. Windbergs, S. Zhou, D. A. Weitz, *Adv. Mater.* **2014**, *26*, 2205.
[67] L. Pauchard, Y. Couder, *EPL* **2004**, *66*, 667.
[68] F. Giorgiutti-Dauphiné, L. Pauchard, *J. Colloid Interface Sci.* **2013**, *395*, 263.
[69] T. Yang, Ph.D. thesis, KTH Royal Institute of Technology, **2012**.
[70] G. Munglani, F. K. Wittel, R. Vetter, F. Bianchi, H. J. Herrmann, *Phys. Rev. Lett.* **2019**, *123*, 058002.
[71] R. Zoelly, *Ph.D. Thesis*, ETH Zürich **1915**.
[72] S. Knoche, J. Kierfeld, *Soft Matter* **2014**, *10*, 8358.
[73] S. Knoche, J. Kierfeld, *Eur. Phys. J. E* **2014**, *37*, 62.
[74] A. P. M. Guttenplan, *Ph.D. Thesis*, University of Cambridge, **2018**.
[75] S. Sacanna, W. T. Irvine, P. M. Chaikin, D. J. Pine, *Nature* **2010**, *464*, 575.
[76] S. Tasoglu, E. Diller, S. Guven, M. Sitti, U. Demirci, *Nat. Commun.* **2014**, *5*, 3124.
[77] A. Alcinesio, O. J. Meacock, R. G. Allan, C. Monico, V. R. Schild, I. Cazimoglu, M. T. Cornall, R. K. Kumar, H. Bayley, *Nat. Commun.* **2020**, *11*, 2105.
[78] J. D. Paulsen, E. Hohlfeld, H. King, J. Huang, Z. Qiu, T. P. Russell, N. Menon, D. Vella, B. Davidovitch, *Proc. Natl. Acad. Sci. USA* **2016**, *113*, 1144.
[79] M. Taffetani, X. Jiang, D. P. Holmes, D. Vella, *Proc. Math. Phys. Eng. Sci.* **2018**, *474*, 20170910.
[80] M. W. Tibbitt, C. B. Rodell, J. A. Burdick, K. S. Anseth, *Proc. Natl. Acad. Sci. USA* **2015**, *112*, 14444.
[81] Y. Jia, Y. Ren, L. Hou, W. Liu, T. Jiang, X. Deng, Y. Tao, H. Jiang, *Lab Chip* **2018**, *18*, 1121.
[82] S. Sindhwani, A. M. Syed, J. Ngai, B. R. Kingston, L. Maiorino, J. Rothschild, P. MacMillan, Y. Zhang, N. U. Rajesh, T. Hoang, J. L. Y. Wu, S. Wilhelm, A. Zilman, S. Gadde, A. Sulaiman,

B. Ouyang, Z. Lin, L. Wang, M. Egeblad, W. C. W. Chan, *Nat. Mater.* **2020**, *19*, 566.
[83] C.-Y. Wu, M. Ouyang, B. Wang, J. de Rutte, A. Joo, M. Jacobs, K. Ha, A. L. Bertozzi, D. Di Carlo, *Sci. Adv.* **2020**, *6*, eabb9023.
[84] H. Chen, Y. Zhao, J. Li, M. Guo, J. Wan, D. A. Weitz, H. A. Stone, *Lab Chip* **2011**, *11*, 2312.
[85] I. Alshareedah, M. M. Moosa, M. Raju, D. A. Potoyan, P. R. Banerjee, *Proc. Natl. Acad. Sci. USA* **2020**, *117*, 15650.
[86] A. A. André, E. Spruijt, *Int. J. Mol. Sci.* **2020**, *21*, 5908.
[87] D. C. Duffy, J. C. McDonald, O. J. A. Schueller, G. M. Whitesides, *Anal. Chem.* **1998**, *70*, 4974.